The *Arabidopsis* Dynamin-Related Protein2 Family Is Essential for Gametophyte Development [C][W]

Steven K. Backues,[a] David A. Korasick,[b] Antje Heese,[b] and Sebastian Y. Bednarek[a,1]

[a] Department of Biochemistry, University of Wisconsin, Madison, Wisconsin 53706
[b] Division of Biochemistry, Interdisciplinary Plant Group, University of Missouri, Columbia, Missouri 65211

Clathrin-mediated membrane trafficking is critical for multiple stages of plant growth and development. One key component of clathrin-mediated trafficking in animals is dynamin, a polymerizing GTPase that plays both regulatory and mechanical roles. Other eukaryotes use various dynamin-related proteins (DRP) in clathrin-mediated trafficking. Plants are unique in the apparent involvement of both a family of classical dynamins (DRP2) and a family of dynamin-related proteins (DRP1) in clathrin-mediated membrane trafficking. Our analysis of *drp2* insertional mutants demonstrates that, similar to the DRP1 family, the DRP2 family is essential for *Arabidopsis thaliana* development. Gametophytes lacking both *DRP2A* and *DRP2B* were inviable, arresting prior to the first mitotic division in both male and female gametogenesis. Mutant pollen displayed a variety of defects, including branched or irregular cell plates, altered Golgi morphology and ectopic callose deposition. Ectopic callose deposition was also visible in the pollen-lethal *drp1c-1* mutant and appears to be a specific feature of pollen-defective mutants with impaired membrane trafficking. However, *drp2ab* pollen arrested at earlier stages in development than *drp1c-1* pollen and did not accumulate excess plasma membrane or display other gross defects in plasma membrane morphology. Therefore, the *DRP2* family, but not *DRP1C*, is necessary for cell cycle progression during early gametophyte development. This suggests a possible role for DRP2-dependent clathrin-mediated trafficking in the transduction of developmental signals in the gametophyte.

INTRODUCTION

Clathrin-mediated endocytosis (CME) plays a number of critical roles in plant development, including retrieval of excess membrane material during tip-directed growth and cell plate maturation (Derksen et al., 1995; Blackbourn and Jackson, 1996; Otegui et al., 2001; Seguí-Simarro et al., 2004) and maintenance of the polar localization of auxin transporters necessary for proper establishment of auxin gradients (Dhonukshe et al., 2007). One critical component of CME in animals is dynamin, a polymerizing GTPase that plays both early regulatory and late mechanical roles (Pucadyil and Schmid, 2008). Dynamin also plays less well-characterized roles in caveolar endocytosis (Henley et al., 1998; Oh et al., 1998; Yao et al., 2005), clathrin-mediated membrane trafficking at the Golgi (Jones et al., 1998), actin dynamics (Orth and McNiven, 2003), and cytokinesis (Konopka et al., 2006). In plants, two separate families of dynamin-related proteins, the dynamin-related protein1 (DRP1) family and the DRP2 family, appear to function in clathrin-mediated membrane trafficking (Bednarek and Backues, 2010).

The DRP1 family contains five members, DRP1A-E, all of which lack the membrane binding pleckstrin homology domain and protein-interacting Pro-rich domain that characterize classical dynamins. Nevertheless, recent localization studies and analyses of DRP1 null mutants indicate that the DRP1 family functions in CME. DRP1A and DRP1C colocalize with clathrin light chain at dynamic plasma membrane (PM) foci thought to represent sites of CME (Konopka and Bednarek, 2008; Konopka et al., 2008). Both DRP1A and DRP1C also localize strongly to the forming cell plate during cytokinesis (Kang et al., 2003a; Konopka et al., 2008). *drp1a* mutant plants are characterized by defects in cell expansion and cell wall deposition in various tissues and cell types (Kang et al., 2001; Kang et al., 2003a; Collings et al., 2008), while *drp1a drp1e* double mutants are embryonic lethal and display cytokinetic as well as expansion defects (Kang et al., 2003a). *drp1c-1* mutants have male gametophytic lethality that manifests late in pollen development as an accumulation and disorganization of PM and internal membranes and eventually leads to shriveled, inviable pollen (Kang et al., 2003b).

The DRP2 family in *Arabidopsis thaliana* consists of two members, DRP2A and DRP2B, that share 93% amino acid sequence identity. These plant DRP2s have a domain structure and organization similar to that of animal dynamin and as such represent the classical dynamins in plants (Figure 1A). Evidence for the function of the DRP2 family in CME includes the interaction of DRP2s with putative CME accessory proteins via their Pro-rich domains (Lam et al., 2002), immuno-transmission electron microscopy (immuno-TEM) localization of DRP2A to PM-associated clathrin-coated structures (Lam et al., 2002), and the
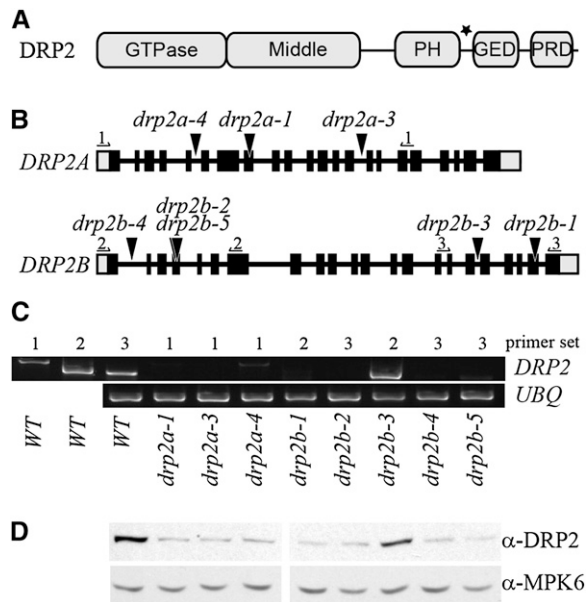
Figure 1. *drp2* Insertional Alleles.

(A) Diagram of DRP2 protein domains. PH, pleckstrin homology (membrane binding); GED, GTPase effector domain; PRD, Pro-rich domain (binds SH3 domain-containing proteins). Middle and GED are coiled-coil domains presumably involved in polymerization. The black star indicates the position of the peptide used for antibody generation.

(B) Position of insertional alleles for *DRP2A* and *DRP2B* (black triangles) and primers used for RT-PCR (numbered arrows) relative to exons (black bars), introns (black lines), and untranslated regions (gray bars).

(C) RT-PCR demonstrating that all alleles except *drp2b-3* produce little to no transcript. RNA was extracted from seedling tissue of the indicated homozygous genotype, reverse transcribed, and amplified with primers flanking the insertion site (primer set), as shown in **(B)**. Control primers against *UBIQUITIN10* (*UBQ*) were used to verify equal loading of all samples. Image is representative of ≥2 technical replicates on each of two separately generated tissue samples. *WT*, wild type.

(D) Immunoblot verifying that all alleles except *drp2b-3* have reduced total levels of DRP2, consistent with a complete loss of DRP2A or DRP2B. Total cellular extracts from seedlings homozygous for the indicated genotype were probed with antibodies raised against a peptide common to both DRP2A and DRP2B. Extracts were also probed with anti-MPK6 to demonstrate equal loading.

localization of DRP2B-GFP (for green fluorescent protein) to dynamic PM foci that colocalize with clathrin light chain-mOrange PM foci (Fujimoto et al., 2010). DRP2B-GFP also localizes to forming cell plate (Fujimoto et al., 2008). The significant colocalization observed between members of the DRP1 and DRP2 family at various subcellular structures (Fujimoto et al., 2008, 2010) raises the question of whether these two structurally distinct families of DRPs play redundant or distinct roles in clathrin-mediated membrane trafficking and plant development.

In this study, we show that *drp2ab* double mutants undergo an early developmental arrest prior to the first mitotic cell division during both male and female gametophytic development, resulting in gametophytic lethality. Therefore, although both the DRP1 and the DRP2 families are involved in endocytosis (Fujimoto

et al., 2010), they do not play redundant roles. Instead, both are independently essential for plant development. In contrast with *drp1* mutants, *drp2ab* did not show plasma membrane morphology defects, suggesting that the DRP2 family of classical dynamins have a different function in clathrin-mediated membrane trafficking than the DRP1 family of DRPs.

RESULTS

Identification of *drp2* Loss-of-Function Mutants

To determine the function of *DRP2A* and *DRP2B* in *Arabidopsis* development, we characterized several independent lines containing T-DNA insertions in *DRP2A* or *DRP2B*. The position of the T-DNA in each line was verified by PCR amplification using gene-specific and T-DNA–specific primers followed by DNA sequencing of the PCR product (Figure 1B). To identify *drp2* null mutant lines, we examined *DRP2A* and *DRP2B* transcript accumulation and DRP2 protein levels in the wild type and each T-DNA insertional line. RT-PCR analysis indicated that all *drp2a* and *drp2b* alleles except *drp2b-3* (which was not further analyzed) accumulated little to no detectable *DRP2A* and *DRP2B* transcript, respectively (Figure 1C). A polyclonal anti-DRP2 antibody generated against a peptide present in both DRP2A and DRP2B was used for immunoblot analysis of total protein extracts from *drp2* seedlings. Lack of either *DRP2A* or *DRP2B* transcript correlated with a reduction in DRP2 protein levels (Figure 1D). No obvious growth or developmental defects were observed in any single mutant.

To examine the genetic interaction between *DRP2A* and *DRP2B*, crosses between homozygous *drp2a* and *drp2b* plants were generated. F1 progeny from the crosses were allowed to self-fertilize, and the genotype of F2 progeny was determined by PCR. Neither homozygous *drp2aabb* plants nor any plants heterozygous for one allele and homozygous for the other (*drp2Aabb* or *drp2aaBb*) were recovered. The same results were obtained for all combinations of *drp2a* and *drp2b* null alleles tested (Table 1), indicating a fully penetrant, synthetic transmission defect of *drp2a* and *drp2b* through both the male and the female gametes.

To verify the observed transmission defects, we performed reciprocal crosses between *DRP2A/drp2a-1; DRP2B/drp2b-2* plants and wild-type plants. When wild-type pollen was used to fertilize *drp2AaBb* ovaries, no progeny (0/120) with the *drp2AaBb* genotype were recovered. Similarly, when *drp2AaBb* pollen was used to fertilize wild-type ovaries, only one *drp2AaBb* plant out of 198 progeny was recovered (see Supplemental Table 1 online). Together, these data demonstrate a near-complete defect in the simultaneous transmission of *drp2a* and *drp2b* alleles through both the male and the female gametes, suggesting that *drp2ab* mutant gametes are inviable.

Development of *drp2ab* Embryo Sacs Is Arrested Prior to Mitosis

Mature, dry siliques from *DRP2A/drp2a-1; DRP2B/drp2b-2* plants were found to have ~25% empty spaces compared

Table 1. *drp2* Segregation Distortion

| Genotype	Wild Type	drp2AABb or drp2AaBB	drp2AaBb or drp2AaBb	drp2AAbb or drp2aaBB	drp2Aabb or drp2aaBb	drp2aabb	n
Expected %	≤6	≤25	≥25	≥12.5	≤25	≤6	
DRP2A/drp2a-1; DRP2B/drp2b-2	4	18	34	44	0	0	140
DRP2A/drp2a-1; DRP2B/drp2b-4	14	29	30	27	0	0	77
DRP2A/drp2a-3; DRP2B/drp2b-2	6	39	29	25	0	0	85

Heterozygous double mutant plants (left column) were allowed to self-fertilize, and the genotype of their progeny (top row) was determined by PCR amplification using allele-specific primers. Percentage of offspring recovered from each genotypic class is indicated and compared to the percentage that would be expected if there were no defects in transmission or viability. The ≤ and ≥ symbols reflect potential minor deviations from the expected percentages due to the possibility of a small degree of linkage between *DRP2A* and *DRP2B*, which are found on opposite arms of chromosome 1.

with <5% empty spaces in wild-type, *drp2a-1/drp2a-1*, and *drp2b-2/drp2b-2* siliques. Small white stubs were observed in empty spaces in maturing *drp2AaBb* siliques, suggesting an early abortion of the mutant ovules (Figure 2). This aborted ovule phenotype was observed in all heterozygous combinations of *drp2a* and *drp2b* null alleles tested (Table 2), consistent with a failure in female gametophyte (embryo sac) development in the ≤25% of ovules expected to contain *drp2ab* gametophytes.

To determine the stage at which *drp2ab* gametophytes deviated from normal embryo sac development, we used laser scanning confocal microscopy to view chemically fixed and propidium iodide–stained pistils from wild-type and *DRP2A/drp2a-1; DRP2B/drp2b-2* plants at various stages of development. Developing embryo sacs were identified by the large size of their cells and nuclei and their position at the center of the ovule, surrounded by two layers of integuments. The number and arrangement of the nuclei in each embryo sac allowed the determination of its female gametophyte (FG) developmental stage, FG1-FG7, based upon the nomenclature of Christensen et al. (1997). Female gametophyte development begins with the postmeiotic degeneration of three of the megagametophytes, leaving only one functional gametophyte. This single-nucleate (FG1) gametophyte undergoes nuclear division without cell division to give rise to the double-nucleate FG2 stage (Figure 3). The nuclei migrate to the opposite ends of the embryo sac syncytium and a large vacuole forms between them, defining the FG3 stage (Figure 3A). Two more rounds of nuclear division (stage FG4) are followed by cellularization (stage FG5). Fusion of the two polar nuclei leads to the seven-nucleate, seven-celled embryo sac (stage FG6) containing an egg cell, two synergids, a central cell and three antipodals (Figure 3A). Degeneration of the three antipodals yields the final four-celled embryo sac (stage FG7), which is ready for fertilization (Christensen et al., 1997).

Consistent with previous reports (Christensen et al., 1997), development of the embryo sac in wild-type pistils was relatively synchronous, with only one or two developmental stages represented within a single pistil (Figures 3B to 3D). At stage FG1, embryo sacs in wild-type and *drp2AaBb* pistils looked identical (Figures 3B and 3E), and most (116/171) embryo sacs in *drp2AaBb* pistils were indistinguishable from the wild type throughout development. However, 55/171 ovules in *drp2AaBb*

pistils at later stages of development contained only a small, single-celled embryo sac with a single prominent nucleus, morphologically identical to wild-type embryo sacs at the FG1 stage of development (Figures 3F and 3G; compare with Figure 3B). FG1-arrested embryo sacs were seen in *drp2AaBb* pistils at all stages of development up to and including early postfertilization (Figure 3G), after which the entire ovule appeared to degenerate. Normally developing and FG1-arrested were the only two embryo sac phenotypes seen in *drp2AaB* pistils; embryo sacs were not observed to arrest at any other developmental stage. Light microscopy of toluidine blue–stained semithin sections from high-pressure frozen, freeze-substituted, and embedded
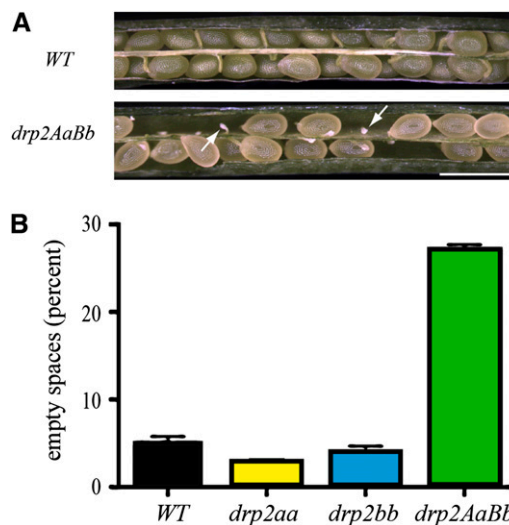
Figure 2. *drp2AaBb* Siliques Have ∼25% Aborted Ovules.

(A) Immature siliques from wild-type (*WT*).
and *DRP2A/drp2a-1; DRP2B/drp2b-2* plants. Arrows indicate empty spaces with aborted ovules. Bar = 1 mm.
(B) Quantification of empty spaces in mature, dry siliques from wild-type, *drp2a-1/drp2a-1*, *drp2b-2/drp2b-2*, and *DRP2A/drp2a-1; DRP2B/drp2b-2* plants. Mean ± SE empty spaces for *n* = 67 siliques is plotted. [See online article for color version of this figure.]

Table 2. *drp2AaBb* Plants Have Shriveled Pollen and Failed Ovules

Genotype	% Shriveled	n	≥5 Failed Ovules?
Wild type	0.7	2165	No
drp2a-1/drp2a-1	1.4	1547	No
drp2a-3/drp2a-3	0.2	1334	No
drp2a-4/drp2a-4	0.1	716	No
drp2b-2/drp2b-2	0.1	1153	No
drp2b-4/drp2b-4	0.0	870	No
drp2b-5/drp2b-5	0.6	1045	No
DRP2A/drp2a-1; DRP2B/drp2b-2	21.6	3841	Yes
DRP2A/drp2a-1; DRP2B/drp2b-4	15.9	2222	Yes
DRP2A/drp2a-1; DRP2B/drp2b-5	13.3	1645	Yes
DRP2A/drp2a-3; DRP2B/drp2b-2	22.9	1042	Yes
DRP2A/drp2a-3; DRP2B/drp2b-4	16.1	2739	Yes
DRP2A/drp2a-3; DRP2B/drp2b-5	16.2	1502	Yes
DRP2A/drp2a-4; DRP2B/drp2b-2	13.9	1472	Yes
DRP2A/drp2a-4; DRP2B/drp2b-4	12.2	1129	Yes
DRP2A/drp2a-4; DRP2B/drp2b-5	18.3	1259	Yes

Mature pollen from open flowers was collected and normal and shriv-eled grains counted by light microscopy. Maturing siliques were dis-sected and viewed under a dissecting microscope to look for significant numbers of failed ovules (≥5 failed ovules/silique). All data represent at least two independent plants of the indicated genotype.

DRP2A/drp2a-1; DRP2B/drp2b-2 pistils verified the presence of FG1-arrested embryo sacs (Figures 3H and 3I). Arrested embryo sacs could be identified by the lack of a large central vacuole (V) found in normally developing embryo sacs at stage FG3 and later.

Arrested *drp2ab* Embryo Sacs Show No Defects in Membrane or Cellular Morphology

drp1a and *drp1c* null mutants show defects in plasma membrane morphology (Kang et al., 2003a, 2003b) and cell wall deposition (Collings et al., 2008), consistent with the proposed role of the DRP1 family in endocytosis. TEM analysis of FG1-arrested embryo sacs in *drp2AaBb* pistils revealed no defects in plasma membrane structure or any other visible defects in subcellular morphology (*n* = 7). Instead, the *drp2ab* embryo sacs arrested at FG1 were similar in appearance to wild-type embryo sacs at the FG1 stage of development (Figure 4).

Together, these results demonstrated that development of *drp2ab* embryo sacs is quantitatively arrested at the single-nucleate FG1 stage, without apparent defects in subcellular morphology.

drp2AaBb Plants Produce Shriveled, Inviable Pollen

Because we observed a transmission defect through both the male and the female gametes (see Supplemental Table 1 online), we next characterized pollen development in the *drp2AaBb* double mutant. Consistent with a defect in male gametophyte development, ∼20% of released pollen grains from *drp2AaBb* anthers were visibly small and shriveled (Figure 5A). The per-centage of pollen that was visibly shriveled varied from ∼10 to

∼25% between individual plants, suggesting that environmental conditions may play a role in the manifestation of this phenotype. Identical phenotypes were observed in all combinations of *drp2a* and *drp2b* null alleles tested (Table 2). By contrast, <2% of the pollen was shriveled in either wild-type or single homozygous *drp2* null alleles (Figure 5B, Table 2). Alexander staining of mature, released pollen from *DRP2A/drp2a-1; DRP2B/drp2b-2* anthers verified that the shriveled pollen grains were inviable
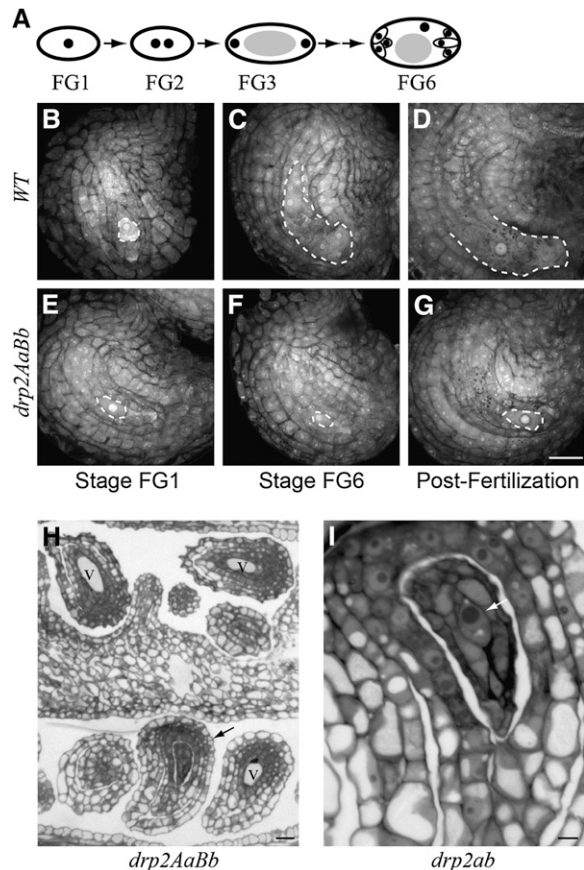

Figure 3. *drp2ab* Embryo Sacs Arrest at the FG1 (Single Nucleate) Developmental Stage.

(A) Diagram of embryo sac development. Black dots indicate nuclei, gray ovals indicate the central vacuole, thin black lines indicate cell bound-aries, and thick black lines indicate the boundary of the gametophyte. *WT*, wild type.

(B) to **(G)** Propidium iodide staining of fixed, dissected ovules from wild-type (**[B]** to **[D]**) and *DRP2A/drp2a-1; DRP2B/drp2b-2* (**[E]** to **[G]**) plants at developmental stages FG1 (**[B]** and **[E]**), FG6 (**[C]** and **[F]**) and shortly after fertilization (**[D]** and **[G]**). Dashed line indicates the border of the embryo sac.

(H) Semithin section through a *DRP2A/drp2a-1; DRP2B/drp2b-2* pistil at stage FG3. Black arrow indicates an ovule with an FG1-arrested embryo sac, as identified by the lack of the large central vacuole (V) found in normally developing gametophytes at stage FG3 and later. Bars = 20 μm in **(B)** to **(H)**.

(I) Higher-magnification view of the arrested ovule indicated in **(H)**. Arrow indicates the boundary of the FG1-arrested embryo sac. Bar = 5 μm.
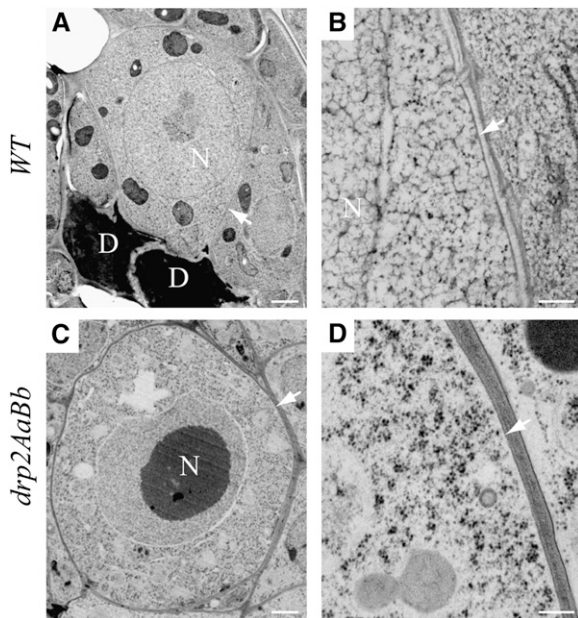
Figure 4. *drp2ab* FG1-Arrested Embryo Sacs Show No Defects in Membrane Morphology.

Wild-type (*WT*) embryo sacs at stage FG1 (**[A]** and **[B]**) were visualized by TEM and compared with FG1-arrested embryo sacs in *DRP2A/drp2a-1; DRP2B/drp2b-2* pistils at stage FG3-FG5 (**[C]** and **[D]**). Arrows indicate the boundary of the FG1 embryo sac. N, nucleus; D, degenerating nonfunctional gametophytes. No defects in membrane structure or cellular organization were visible in the FG1-arrested mutant embryo sacs (*n* = 7 arrested embryo sacs). Bars = 1 µm in **(A)** and **(C)** and 200 nm in **(B)** and **(D)**.

(Figures 5C and 5D). To confirm that the defective pollen phenotype was due to a gametophytic, not sporophytic, defect, the *drp2a-1* and *drp2b-2* alleles were introgressed into the *quartet* (*qrt*) mutant. In this mutant, the four meiotic products of pollen sporogenesis remain associated as a tetrad throughout pollen development (Preuss et al., 1994). Each individual meiotic event results in the production of zero, one, or two *drp2ab* grains depending on the segregation of the chromosomes during meiosis I and whether or not recombination occurred. As expected, tetrads from anthers of *drp2AaBb;qrt/qrt* plants displayed either zero, one, or two shriveled pollen grains (Figures 5E to 5G), supporting the conclusion that the shriveled grains represented *drp2ab* gametes.

Development of *drp2ab* Pollen Is Arrested Prior to Pollen Mitosis I

Wild-type pollen development proceeds through well-defined stages (Figure 6A) (Owen and Makaroff, 1995; Twell et al., 2006; Borg et al., 2009) that can be easily visualized by staining with 4′,6-diamidino-2-phenylindole (DAPI) to follow the number, shape, and position of nuclei. DAPI-stained pollen from *DRP2A/drp2a-1; DRP2B/drp2b-2* anthers appeared normal during the tetrad (Figure 6B) and released microspore (Figure 6C)

stages of development. Microspore polarization also proceeded without visible defect (Figure 6D). However, by the early bicellular stage, some pollen grains were slightly smaller and displayed either aberrant or, more commonly, no DAPI staining (Figure 6E). By the later bicellular stage of development, the difference in size between the normal and mutant grains was readily distinguishable (Figure 6F). Defects in the overall integrity of the pollen grain were increasingly apparent in tricellular (Figure 6G) and mature (Figure 6H) pollen.

To further examine *drp2ab* pollen development, wild-type and *DRP2A/drp2a-1; DRP2B/drp2b-2* anthers were high-pressure frozen, freeze-substituted, and embedded. Pollen in wild-type anthers progressed through development in a synchronized fashion, and no collapsed or otherwise aberrant pollen were observed in toluidine blue–stained anther sections viewed by light microscopy (Figures 6I to 6L). No defects in structural integrity of the pollen were observed in toluidine blue–stained
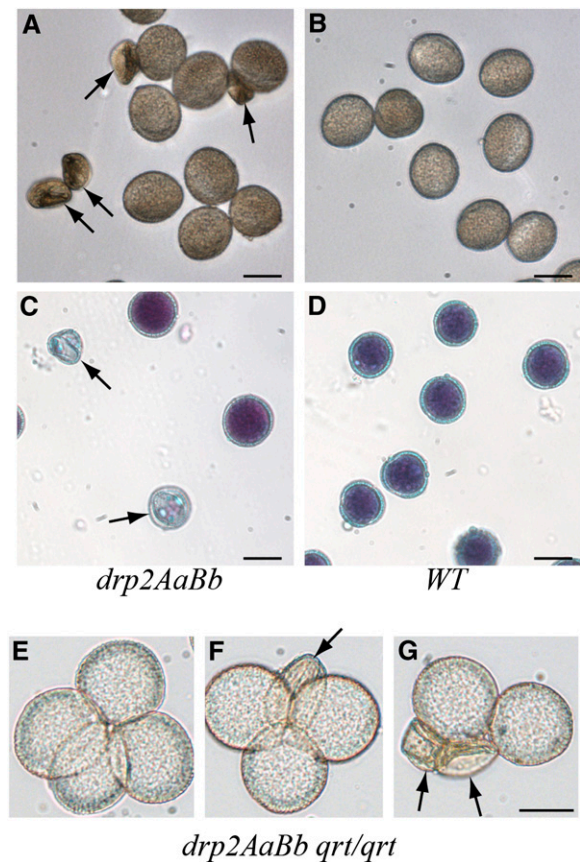

Figure 5. *drp2ab* Pollen Grains Are Shriveled and Inviable.

Mature pollen from *DRP2A/drp2a-1; DRP2B/drp2b-2* (**[A]** and **[C]**) or wild-type (*WT*; **[B]** and **[D]**) anthers visualized by light microscopy (**[A]** and **[B]**) or Alexander staining (**[C]** and **[D]**). Arrows indicate shriveled, inviable grains.

(E) to **(G)** Representative images of pollen quartets from a *DRP2A/drp2a-1; DRP2B/drp2b-2*; *qrt/qrt* mutant. Zero **(E)**, one **(F)**, or two **(G)** shriveled grains were observed per quartet, consistent with a gametophytic defect. Bars = 20 µm.

Table 3. Genotyping of *drp2* Insertional Alleles

drp2 Allele	Line	Insert Position	Left Primer	Right Primer
drp2a-1	SALK_071036	2246	1164	1165
drp2a-3	SALK_011319	3979	1171	1172
drp2a-4	SALK_018859	1374	858	1165
drp2b-1	SALK_003049	7145	865	1056
drp2b-2	SALK_134887	1120	1161	1160
drp2b-3	SALK_124686	6396	861	865
drp2b-4	WISCDSLOX_256E05	255	1162	1163
drp2b-5	SALK_041330	1305	1160	1161

The T-DNA insert was detected by PCR amplification of total genomic DNA preps using a T-DNA primer (774 for line *drp2b-4* and 926 for all other lines) in combination with the left primer; the absence of the insert (to distinguish heterozygous from homozygous plants) was detected by amplification using the left and right primers. The exact position of the insert (number of bases 5′ of ATG in genomic sequence) was determined by direct sequencing of the genotyping PCR reaction. Primer sequences are listed in Supplemental Table 2 online.

sections from *drp2AaBb* anthers at the polarized microspore stage and during pollen mitosis I (Figures 6M and 6N). However, in *drp2AaBb* anthers at the early bicellular stage, we observed grains that had not undergone pollen mitosis I but were instead arrested at the polarized microspore stage, with no evidence of vacuole division or mitotic entry (Figure 6O, arrowhead). Some of these grains were undergoing or had undergone cytoplasmic collapse (Figure 6O, arrow). Both arrested and collapsed pollen were likewise observed in anthers at the tricellular stage, although the proportion of collapsed versus arrested pollen was higher in older anthers, suggesting a progressive collapse of the arrested grains (Figure 6P). The total amount of arrested and collapsed pollen together accounted for ~30 to 35% of all pollen grains at all stages post pollen mitosis I.

Defective Pollen Cell Plates Are Observed in *drp2AaBb* Anthers

The cell plate formed during pollen mitosis I has a characteristic hemispherical shape, forming a cage around the generative nucleus (Heslop-Harrison, 1968; Brown and Lemmon, 1991; Park and Twell, 2001) that appears as a smooth semicircle in toluidine blue–stained sections (Figures 7A and 7B). The majority of dividing pollen grains in *drp2AaBb* anthers had morphologically normal cell plates, but some plates were aberrantly shaped, showing irregular contours (17 out of 139; Figures 7C and 7D) or even possessing branched structures (6 out of 139; Figures 7E and 7F). Abnormal cell plates were also visible in *drp2AaBb* anthers by TEM (Figures 7G to 7L). No cells with persistent cell plates or aberrantly shaped generative nuclei were observed in older, bicellular, *drp2AaBb* anthers.

TEM Analysis of Arrested *drp2ab* Pollen

The ultrastructure of wild-type and *drp2ab* pollen was further examined by TEM to determine the earliest stage at which defects in *drp2ab* development could be seen. We were able to

subdivide the polarized microspore stage of wild-type pollen development into two substages based on the appearance of the intine (the innermost layer of the pollen coat) and the endoplasmic reticulum (ER) in electron micrographs. The early polarized microspore stage was characterized by a thin and completely smooth intine (Figures 8A and 8E, white arrowhead) and the presence of thin, darkly staining ER profiles (Figure 8A, black arrows). By contrast, the late polarized microspore stage, just prior to pollen mitosis I, was characterized by a thicker, convoluted intine containing cytoplasmic inclusions and rounder, lighter staining ER profiles (Figures 8B and 8F). Development of pollen in wild-type anthers was synchronized so that early and late polarized microspores were not found in the same anther. In *drp2AaBb* anthers bearing pollen in the late polarized microspore stage, however, 7/29 microspores appeared to be arrested at the early polarized microspore stage based on intine morphology (see Supplemental Figure 1 online). Three of these arrested grains also contained thin ER profiles. Similarly, in anthers at pollen mitosis I (Figures 8C and 8G), 43/147 grains appeared to be arrested at the early polarized microspore stage, displaying completely smooth intines; 22 of these arrested grains also contained thin ER profiles (Figures 8D and 8H, black arrows).

As seen by bright-field microscopy (Figures 6O and 6P), some arrested pollen persisted into the bicellular stage of development (Figures 8J and 8L), while others collapsed (Figure 8M). About half of these persistent arrested grains (7/17) still displayed thin ER profiles, but 16/17 had a more convoluted intine structure than the arrested grains observed in earlier stages (Figure 8L). However, this intine was often more heterogeneous in appearance than in wild-type grains, and in 7/17 cases contained lightly staining material reminiscent of callose (β-(1,3)-glucan) deposits (Figure 8N). Consistent with this, significant immunoreactivity to an anticallose antibody was seen in 11/12 persistent arrested microspores (Figure 8O) but only 2/20 normally developing siblings (Figure 8P) in a section from a *drp2AaBb* anther at the bicellular stage of development.

On average, Golgi stacks in the persistent arrested microspores of bicellular *drp2AaBb* anthers contained slightly more cisternae and were more variable in morphology than in wild-type grains at the polarized microspore stage (Figures 8R to 8U). Even when stacks with the same number of visible cisternae were compared, Golgi stacks in persistent arrested *drp2AaBb* grains were significantly longer and narrower than in the wild type (Figure 8V), reflecting differences in the dimensions and spacing of the individual cisternae. The same Golgi phenotype, but less severe, was also observed in arrested grains in *drp2AaBb* anthers undergoing pollen mitosis I. No defect in plasma membrane morphology or accumulation of excess plasma membrane or internal membranes was observed in the arrested pollen grains at any stage. Taken together, these results demonstrate that *drp2ab* pollen grains, like *drp2ab* embryo sacs, arrest prior to the first mitotic division without defects in plasma membrane morphology.

drp2ab and *drp1c-1* Pollen Display Ectopic Callose Deposition

Because of the callose staining observed in the intine layer of arrested *drp2ab* microspores, we investigated whether pollen
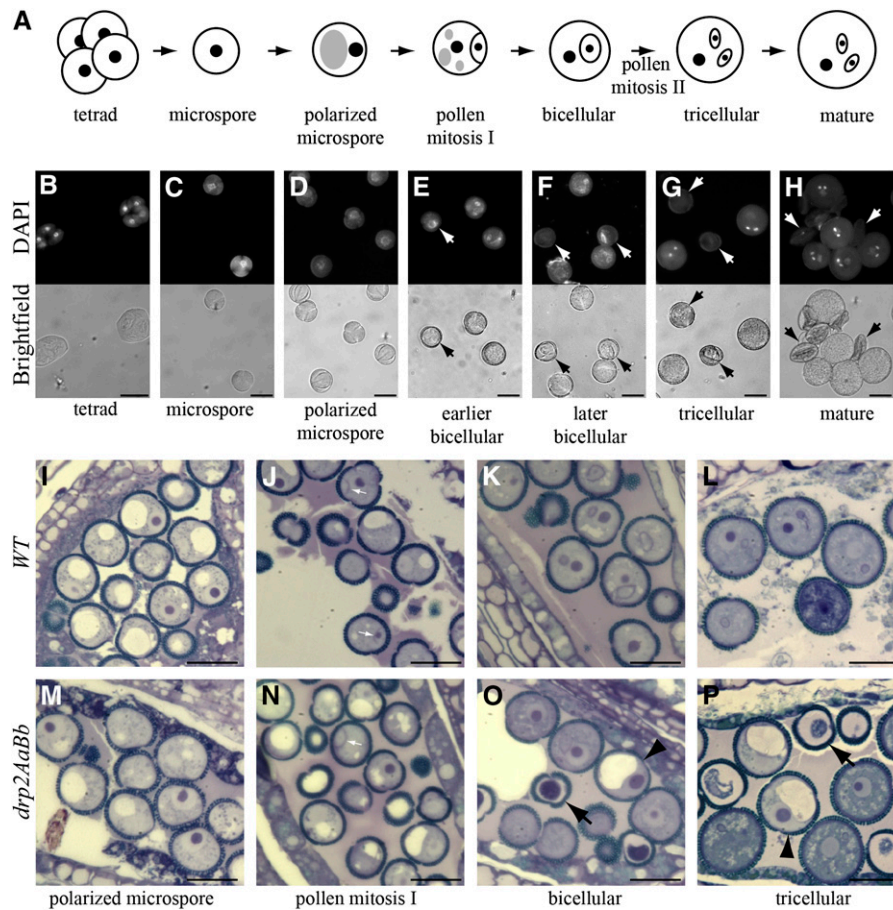
Figure 6. *drp2ab* Pollen Grains Arrest or Collapse at Pollen Mitosis I.

(A) Diagram of pollen sac development. Black dots indicate nuclei, gray ovals indicate vacuoles, and black lines indicate cell boundaries.

(B) to **(H)** Pollen from *DRP2A/drp2a-1; DRP2B/drp2b-2* anthers stained with DAPI to label nuclei and visualized under fluorescent (top row) or bright-field (bottom row) optics. Aberrantly staining or nonstaining grains (arrows) were first observed at the early bicellular stage **(E)** and began showing structural defects by the late bicellular stage **(F)**, eventually giving rise to completely shriveled pollen **(H)**.

(I) to **(P)** Semithin sections through wild-type (*WT*; **[I]** to **[L]**) and *DRP2A/drp2a-1; DRP2B/drp2b-2* (**[M]** to **[P]**) anthers. Collapsing pollen (black arrows) and pollen arrested at the polarized microspore stage (black arrowheads) were observed in *drp2AaBb* anthers by the early bicellular stage **(O)**. White arrows in **(J)** and **(N)** indicate cell plates. Bars = 20 μm in **(B)** to **(P)**.

[See online article for color version of this figure.]

from *DRP2A/drp2a-1; DRP2B/drp2b-2* anthers showed callose deposition at the bicellular and tricellular stages. Consistent with previous reports (Johnson and McCormick, 2001), wild-type pollen showed very little callose deposition at these stages as determined by aniline blue staining (Figures 9A and 9B). By contrast, ~15% of pollen from *DRP2A/drp2a-1; DRP2B/drp2b-2* anthers at the late bicellular stage showed bright callose staining on the surface of the grain (Figures 9C and 9D). The intensity of the staining was variable, and staining was sometimes found in speckles or concentrated at the three apertures of the grain. Brightly stained grains were likewise seen in anthers from *DRP2A/drp2a-4*, *DRP2B/drp2b-4* plants (see Supplemental Figure 2 online) but not in anthers from single homozygous *drp2a-1*, *drp2a-4*, *drp2b-2*, or *drp2b-4* plants. Interestingly, this staining was brightest in anthers at the late bicellular and early

tricellular stages but progressively dimmer in the later tricelluar stage and almost absent in mature, released pollen. To determine if other dynamin mutants also showed ectopic callose deposition, we also stained pollen from *DRP1C/drp1c-1* anthers with aniline blue. A proportion of the pollen from these anthers also displayed bright callose staining at the surface, in speckles, and sometimes in large inclusions in the grain (Figures 9E and 9F). In *drp1c-1* pollen, staining was first observed at the mid-tricellular stage and persisted into mature, released pollen.

To determine whether ectopic callose deposition was a general feature of pollen-lethal mutants, we stained bicellular and tricellular anthers from seven independent pollen lethal mutants. All seven of these mutants displayed visibly shriveled, inviable pollen (see Supplemental Figure 3 online), but only one out of the seven showed significant levels of callose staining at any stage
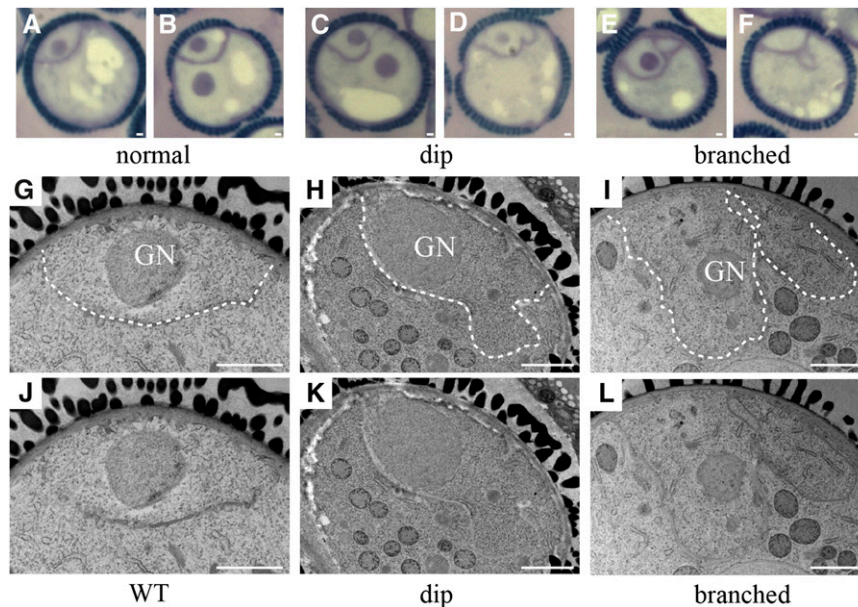
Figure 7. Cell Plate Defects Are Seen in *drp2AaBb* Anthers at Pollen Mitosis I.

(A) to **(F)** Semithin sections of pollen from *DRP2A/drp2a-1; DRP2B/drp2b-2* anthers at pollen mitosis I, showing the range of observed cell plate phenotypes.
(G) to **(L)** TEM images of pollen from wild-type (WT; **[G]** and **[J]**) and *DRP2A/drp2a-1; DRP2B/drp2b-2* (**[H]**, **[I]**, **[K]**, and **[L]**) anthers at pollen mitosis I. GN, generative nucleus. White dotted lines in **(G)** to **(I)** indicate cell plate. Bars = 1 μm.
[See online article for color version of this figure.]

(see Supplemental Figure 4 online). This demonstrates that ectopic callose deposition is not a general feature of all developmentally defective pollen.

DISCUSSION

DRP2A and DRP2B Play Functionally Redundant Roles in Plant Development

DRP2A and DRP2B are 93% identical at the amino acid level, and both are expressed throughout plant development (Bednarek and Backues, 2010), suggesting that they serve redundant functions in plant morphogenesis. Consistent with this, no morphological or developmental defects were observed in single homozygous *drp2a* or *drp2b* mutants. By contrast, Abe et al. (2008) reported an aerial rosette phenotype in 50 to 90% of plants from homozygous *drp2a* (*drp2a-1, drp2a-2,* and *drp2a-3*) and *drp2b* (*drp2b-2* and *drp2b-3*) single mutant lines compared with only in 10% of wild-type plants. We did not observe aerial rosettes in either wild-type or any *drp2a* or *drp2b* mutant plants analyzed in this study, suggesting that different growth conditions may be required for the manifestation of this phenotype.

The DRP2 Family Is Essential for Plant Development

Both the DRP1 and DRP2 families have been implicated in endocytosis (Bednarek and Backues, 2010; Fujimoto et al.,

2010), raising the question of whether these two families play distinct or redundant roles in *Arabidopsis* development. Previous work has shown that members of the DRP1 family are essential for normal PM dynamics and cell plate biogenesis at various stages of growth (Kang et al., 2003a, 2003b; Collings et al., 2008). Here, we show that members of the DRP2 family of DRPs are likewise essential for plant development. Our results demonstrate that both male and female gametes require at least one functioning DRP2 family member to progress beyond the single-nucleate stage of development.

drp2 Pollen Phenotypes Suggest Roles in Membrane Trafficking and Cell Plate Formation

Approximately 30% of pollen grains in *drp2AaBb* anthers at pollen mitosis I are arrested at the early polarized microspore stage of development. This class of arrested grains likely represents the *drp2ab* gametes, known from segregation analyses to be inviable. Arrested *drp2ab* grains show progressive defects in Golgi morphology. These morphological defects were only apparent after the onset of developmental arrest and so cannot be the direct cause of the arrest. Nevertheless, they suggest a role for DRP2 in Golgi maintenance and/or vesicular trafficking. Such a role would be consistent with the reports that DRP2A localizes to the trans-Golgi network (TGN) in pollen (Lam et al., 2002) and functions in TGN-to-vacuole trafficking in protoplasts (Jin et al., 2001).

In addition, 17% of pollen grains undergoing pollen mitosis I in *drp2AaBb* anthers have visible defects in cell plate formation.
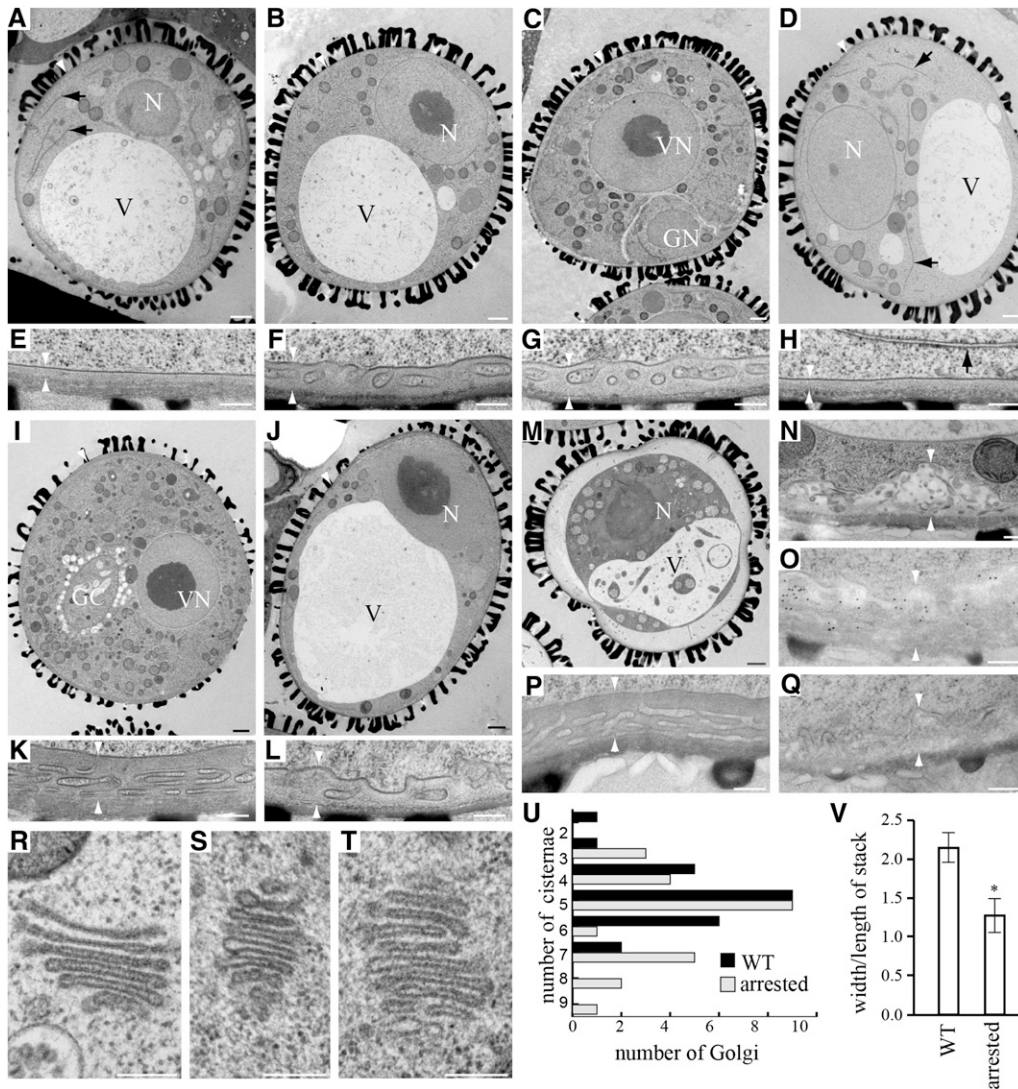
Figure 8. *drp2ab* Pollen Phenotypes.

Pollen in wild-type and *DRP2A/drp2a-1; DRP2B/drp2b-2* anthers visualized by TEM.

(A), **(B)**, **(E)**, and **(F)** Wild-type grains at the early (**[A]** and **[E]**) and late (**[B]** and **[F]**) polarized microspore stage.

(C), **(D)**, **(G)**, and **(H)** Normally developing (**[C]** and **[G]**) and arrested (**[D]** and **[H]**) grains from a *drp2AaBb* anther at pollen mitosis I.

(I) to **(L)** Normally developing (**[I]** and **[K]**) and persistent arrested (**[J]** and **[L]**) grains from a *drp2AaBb* anther at the bicellular stage.

(M) An arrested grain from a *drp2AaBb* anther at the bicellular stage undergoing cytoplasmic collapse.

(N) Abnormal cell wall deposits in persistent arrested grains from a *drp2AaBb* anther at the bicellular stage.

(O) and **(P)** Immunogold labeling of callose deposition in *drp2AaBb* anthers at the bicellular stage with an anti-β-(1,3)-glucan antibody. Significant labeling is seen in the intine of persistent arrested grains **(O)** but not normally developing siblings **(P)**.

(Q) Background control: another section of the persistent arrested grain pictured in **(O)** processed without inclusion of the anti-β-(1,3)-glucan antibody.

(R) Golgi stack from a wild-type pollen grain at the polarized microspore stage.

(S) and **(T)** Golgi stacks from persistent arrested grains in a *drp2AaBb* anther at the bicellular stage.

(U) Graph representing the number of visible cisternae for each Golgi stack in sections of wild-type (WT) grains at the polarized microspore stage and arrested grains in *drp2AaBb* anthers at the bicellular stage.

(V) The average ratio of the maximum width of each Golgi stack versus the length of the entire stack for Golgi with five visible cisternae in sections from wild-type grains at the polarized microspore stage and persistent arrested grains in *drp2AaBb* anthers at the bicellular stage. Mean ± SE for *n* = 9 stacks is plotted. Asterisk indicates P ≤ 0.5 (Student's *t* test).

V, vacuole; N, nucleus; GN, generative nucleus; VN, vegetative nucleus; GC, generative cell. Black arrows in **(A)**, **(D)**, and **(H)** indicate thin, dark ER profiles. White arrowheads in **(A)** to **(L)**, and **(N)** to **(Q)** indicate the intine. Bars = 1 μm in **(A)** to **(D)**, **(I)**, **(J)**, and **(M)** and 200 nm in **(E)** to **(H)**, **(K)**, **(L)**, and **(N)** to **(T)**.
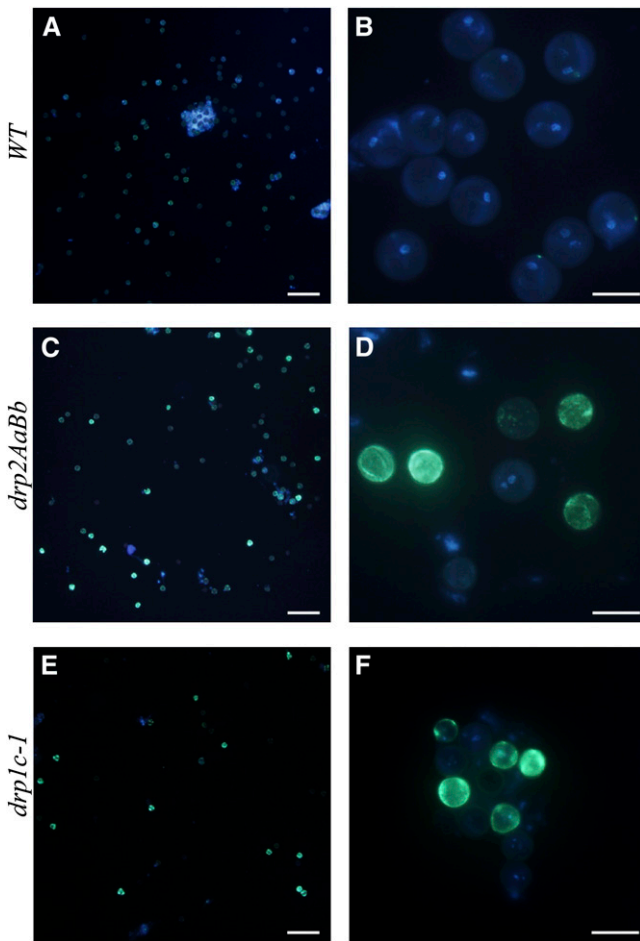
Figure 9. Ectopic Callose Deposition in Pollen from *DRP2A/drp2a-1; DRP2B/drp2b-2* and *P1C/drp1c-1* Anthers.

Pollen from developing wild-type (*WT*; **[A]** and **[B]**), *DRP2A/drp2a-1; DRP2B/drp2b-2* (**[C]** and **[D]**), and *DRP1C/drp1c-1* (**[E]** and **[F]**) anthers stained with DAPI to label nuclei (blue) and aniline blue to detect callose (yellow-green) and visualized under fluorescent optics. Bars = 100 μm in **(A)**, **(C)**, and **(E)** and 20 μm in **(B)**, **(D)**, and **(F)**.

The branched cell plates observed are reminiscent of defects seen in cell plate–defective pollen mutants, such as *gemini pollen I* (Park and Twell, 2001) and *gsl10-1* (Töller et al., 2008). Branched cell plates suggest a role for DRP2 in maintenance of proper cell plate morphology, consistent with its previously reported cell plate localization (Fujimoto et al., 2008). However, unlike in *gemini pollen I* or *gls10-1*, persistent defective cell plates or extra cell walls are not visible at later stages of development. It may be that the aberrant cell plate morphology in these grains does not hinder completion of cytokinesis. Alternatively, the grains with aberrant cell plates may be among those that subsequently abort. The percentage of grains seen with this phenotype (17%, in addition to the 30% that never enter pollen mitosis I) argues for the former explanation and also suggests that those grains with aberrantly formed cell plates may represent singly deficient *drp2Ab* or *drp2aB* gametophytes. However,

further analysis of pollen development in *drp2* single mutants will be necessary to clearly distinguish between these possibilities.

Ectopic Callose Deposition in Pollen Mutants with Defects in Membrane Trafficking

Callose is present at the forming cell plate and at the cell wall during wounding responses but is not a significant component of the mature cell walls in somatic tissue (Chen and Kim, 2009). At the early stages of pollen development, the four pollen grains of a tetrad are held together by a callose wall, which is degraded to release the microspores (Chen and Kim, 2009). Callose is also a major component of pollen cell plates and of the pollen tube cell wall (Ferguson et al., 1998). However, callose is not a significant component of the pollen coat at other stages of pollen development (Johnson and McCormick, 2001). We observed ectopic callose deposition in pollen from both *drp2AaBb* and *DRP1C/drp1c-1* plants. In addition, Van Damme et al. (2006) reported the formation of large ectopic callose deposits in pollen of the *tplate* mutant, which also has a shriveled pollen phenotype. TPLATE has domains similar to those of coat proteins, and like the DRPs, TPLATE may be involved in membrane trafficking during cytokinesis and cell expansion. By contrast, only one out of seven uncharacterized pollen lethal mutants had significant amounts of callose staining. This demonstrates that ectopic callose deposition is not a general feature of disrupted pollen development, but instead a phenotype specific to a subclass of pollen mutants, and may be indicative of mutants with defects in membrane trafficking pathways.

An aniline blue staining screen for pollen mutants with ectopic callose deposition has been previously performed by Johnson and McCormick (2001). In addition to pollen with a precocious germination phenotype, they found mutants with intense spots of callose (*polka dot pollen*) and diffuse callose staining over the surface of the grain (*emotionally fragile pollen*). Based on the similar staining patterns seen in *tplate*, *drp1c-1*, and *drp2ab* pollen, we speculate that these as yet uncharacterized mutants may also prove to have defects in membrane trafficking or cell wall deposition pathways.

drp2ab and *drp1* Mutants Show Distinct Membrane Defects

Arrested *drp2ab* pollen show phenotypes consistent with a possible role of the DRP2 family in membrane trafficking. However, the *drp2ab* phenotypes are distinct from membrane trafficking defects observed in the *drp1* mutants. While both *drp2ab* and *drp1c-1* pollen display developmental defects, the defect in *drp1c-1* pollen does not manifest itself until the bicellular stage (Kang et al., 2003b). *drp1c-1* pollen also show a profound disorganization and accumulation of PM, similar to that seen in failed stigmatic papillae cells in the *drp1a-2* mutant (Kang et al., 2003a, 2003b). By contrast, PM morphology defects are not seen in either arrested *drp2ab* pollen grains or arrested *drp2ab* embryo sacs.

One possible interpretation of these results is that DRP2 functions preferentially at the TGN, whereas DRP1 functions primarily at the plasma membrane. However, the localization of DRP1 and DRP2B in *Arabidopsis* roots is strikingly similar: both proteins are concentrated at the PM and cell plate, with the

occasional appearance of cytoplasmic puncta resembling TGN (Kang et al., 2003a; Fujimoto et al., 2007; Konopka et al., 2008). In addition, DRP2B-GFP and DRP1A-mOrange show a high degree of colocalization in dynamic PM-associated foci in *Arabidopsis* suspension-cultured cells, suggesting that these two proteins work together at sites of endocytosis (Fujimoto et al., 2010). In protoplasts, both DRP2A (Jin et al., 2001) and DRP1A (Sawa et al., 2005) localize primarily to the TGN. Taken together, these localization studies suggest that DRP2 and DRP1 function at the same sites in the cell. Nevertheless our genetic analyses suggest that DRP2 and DRP1 have distinct (although possibly overlapping or partially redundant) developmental functions. Therefore, it remains to be determined whether DRP1 and DRP2 operate synergistically, antagonistically, or in parallel in clathrin-mediated membrane trafficking.

Role of the DRP2 Family in Gametophyte Development

DRP2, but not DRP1C, is required for cell cycle progression in the early gametophyte, as demonstrated by the arrest of *drp2ab* gametophytes prior to the first mitotic division. In *drp2ab* pollen, this arrest occurs prior to the manifestation of any defects in subcellular morphology. Other cell cycle regulation mutants with gametophytic defects have been described, including the RING-type E3 ligase *rhf1a rhf2a* double mutant, which shows a partially penetrant FG1 embryo sac arrest as well as a partially penetrant pollen arrest prior to both pollen mitosis I and pollen mitosis II (Liu et al., 2008). Progression of the gametophyte through the first mitotic division is also under transcriptional control. Embryo sacs in *agl23* mutants, which are defective for a putative MADS box transcription factor, show a partially penetrant FG1 arrest (Colombo et al., 2008). Both embryo sacs and pollen show a partially penetrant arrest prior to the first mitosis in *ham1 ham2* double mutants, which encode plant-specific histone-acetyl transferases (Latrasse et al., 2008). In both the *rhf1a rhf2a* and the *ham1 ham2* double mutants, the arrested embryo sacs appeared to persist within the ovule, whereas the arrested pollen collapsed. This matches the phenotype seen by both light and electron microscopy in the *drp2AaBb* mutants, suggesting that it (the similar phenotypes) may reflect a general difference in pollen versus embryo sac development.

How might DRP2, a classical dynamin with putative roles in membrane trafficking, affect cell cycle progression? One possibility is that DRP2-mediated membrane trafficking functions in the perception of an extracellular signal necessary for progression of gametophytic development. Gametophyte development occurs while surrounded by maternal tissue, and there is evidence for signaling between the gametophyte and the sporophyte. For example, specific arabinogalactan proteins label the cell surface of gametophytic and adjacent sporophytic tissue during both male and female gametophyte development (Coimbra et al., 2007), and RNA interference depletion of the arabinogalactan protein *APG18* causes an FG1 embryo sac arrest (Acosta-García and Vielle-Calzada, 2004). Also, mutants in a putative sensor His kinase, CKI1, show embryo sac developmental defects beginning at stage FG4 (Pischke et al., 2002; Hejátko et al., 2003). Auxin signaling has also been implicated in cell cycle regulation in many tissues, including gametophytes. In

a *tir1 afb1 afb2 afb3* quadruple auxin perception mutant, 26/399 embryo sacs arrested at stage FG1 (Pagnussat et al., 2009). This same auxin perception mutant actually shows accelerated pollen development (Cecchetti et al., 2008), consistent with the idea that auxin plays tissue type–specific roles in cell cycle regulation (del Pozo et al., 2005).

Membrane trafficking is necessary for the maintenance of auxin gradients in many tissues of the plant (Steinmann et al., 1999; Geldner et al., 2003; Dhonukshe et al., 2007, 2008) as well as for the localization and signaling of receptors for some plant hormones, such as brassinosteroids (Geldner et al., 2007). Arabinogalactan proteins also undergo endocytosis (Herman and Lamb, 1992), although it is not known what role their internalization plays in signaling.

Although a role for DRP2 in perception or regulation of a maternal or other extracellular signal necessary for gametophyte development is speculative, it is consistent with the observed phenotype of the *drp2ab* pollen and embryo sacs: a selective arrest prior to the first mitosis with few visible defects in cell morphology, in contrast with the somewhat later and more variable arrest seen in female gametophyte mutants defective in basic cellular functions (Pagnussat et al., 2009). However, more work needs to be done to understand what signaling pathways are active during gametophyte development and whether these pathways are dependent on clathrin-mediated membrane trafficking at the PM and/or the Golgi complex or whether DRP2 plays a distinct developmental role.

METHODS

Unless otherwise noted, all materials and reagents were purchased from Fisher Scientific. Oligonucleotides were purchased from Integrated DNA Technologies.

Seeds were sterilized with 70% ethanol + 1% (v/v) Triton X-100 for 5 min followed by 1 min in 95% ethanol and plated on solid media containing 0.5× Murashige and Skoog salts (Caisson Labs) and 0.6% agar (Sigma-Aldrich). Plates were stratified for 3 d at 4°C before germination for 5 to 7 d in continuous light. Seedlings were transplanted to Metro Mix 360 potting soil (Sun Gro) and grown under 16-h-light/8-h-dark conditions at 24°C.

Insertional alleles were acquired from the ABRC (Columbus, Ohio) and verified by PCR-based genotyping (Table 3). Wild-type and all insertional alleles were of the Columbia ecotype. Genomic DNA extraction for genotyping was performed in a 96-well format essentially as by Michaels and Amasino (2001). RNA extraction from equal masses of powder from liquid N2-frozen wild-type and mutant seedling was performed with TRIzol reagent (Invitrogen) according to the manufacturer's protocol, and reverse transcription was performed using a MLV-RT kit from Promega. Equal loading of the resulting cDNA was verified using primers 747 and 748 (see Supplemental Table 2 online), specific for *UBIQUITIN10*. Gene-specific transcripts were detected using a primer pair flanking the insertional site (Figure 1B). Primers 968 and 859 were used for all *drp2a* alleles, primers 964 and 1056 were used for *drp2b-1* and *2b-3*, and primers 962 and 1055 were used for *drp2b-2*, *2b-4*, and *2b-5* (see Supplemental Table 2 online). PCR amplification was performed under saturating conditions (e.g., 40 cycles) and visualized using ethidium bromide after separation on an agarose gel to give a qualitative result regarding the presence or absence of a given transcript.

The DRP2 peptide *CQSLSEGSLDKMVRK*, found between the pleck-strin homology and GED domains (Figure 1A), was used for antibody

production in rabbits and subsequent peptide affinity purification according to the company's specifications (Sigma Genosys). Immunoblot analysis of seedling extracts was basically performed as described (Heese et al., 2007) with α-DRP2 used at 1:3000 and α-MPK6 (Heese et al., 2007) at 1:3000.

For determination of female gametophyte developmental stage, whole floral rosettes were chemically fixed and cleared in 70% (v/v) ethanol. Excised pistils were stained 16 h with 0.1 mg/mL propidium iodide, and dissected ovules were viewed by laser scanning confocal microscopy. Pollen was isolated by vortexing four to six open flowers in 500 μL pollen isolation buffer (PIB; 100 mM NaPO$_4$, pH 7.5, 1 mM EDTA, and 0.1% [v/v] Triton X-100) followed by centrifugation for 30 s at 1500g. Isolated pollen was counted on a hemocytometer. For pollen staining, fresh anthers were squashed in 3 μg/mL DAPI in PIB to visualize nuclei, 3 μg/mL DAPI and 0.1% w/v aniline blue in PIB to visualize nuclei and callose, or Alexander Stain (Bonhomme et al., 1999) to test viability.

Samples for bright-field microscopy and TEM were high-pressure frozen and substituted with 2% OsO$_4$ in 100% acetone and infiltrated with Epon resin as described by Otegui et al. (2001). Toluidine blue staining was performed on 1-μm-thick sections, and TEM was performed on 90-nm sections. For immune-electron microscopy detection of callose, sections were first treated for 10 min with NaIO$_4$ (saturated aqueous) to remove OsO$_4$ and then immunolabeled using mouse monoclonal anti-β-(1,3)-glucan antibodies (Biosupplies Australia) followed by F(ab')2 goat anti-mouse conjugated to 15-nm gold particles (Electron Microscopy Sciences) as described by Boudjeko et al. (2006).

Pollen lethal mutants for aniline blue staining were a generous gift of Katie Davis of the Patrick Krysan lab (University of Wisconsin, Madison). These mutants are the F1 progeny of crosses between wild-type Landsberg *erecta* plants and seven independent Salk insertional alleles that display pollen lethality upon outcrossing. This lethality is likely due to reciprocal chromosomal translocations in the parental Salk allele that cause 50% of the outcrossed pollen to have large chromosomal deletions that lead to pollen lethality, as has been previously described (Curtis et al., 2009).

Accession Numbers

Sequence data from this article can be found in the Arabidopsis Genome Initiative or GenBank/EMBL databases under accession numbers At1g10290 (*DRP2A*) and At1g59610 (*DRP2B*).

Supplemental Data

The following materials are available in the online version of this article.

Supplemental Figure 1. *drp2ab* Pollen Grains Arrest at the Polarized Microspore Stage.

Supplemental Figure 2. Ectopic Callose Deposition in Pollen from *DRP2A/drp2a-4; DRP2B/drp2b-4* Anthers.

Supplemental Figure 3. Alexander Staining of Pollen Lethal Mutants.

Supplemental Figure 4. Aniline Blue Staining of Pollen Lethal Mutants.

Supplemental Table 1. Analysis of Progeny from *drp2AaBb/WT* Reciprocal Crosses.

Supplemental Table 2. Oligonucleotides Used in This Study.

REFERENCES

Abe, M., Fujiwara, M., Kurotani, K., Yokoi, S., and Shimamoto, K. (2008). Identification of dynamin as an interactor of rice GIGANTEA by tandem affinity purification (TAP). Plant Cell Physiol. **49:** 420–432.

Acosta-García, G., and Vielle-Calzada, J.P. (2004). A classical arabinogalactan protein is essential for the initiation of female gametogenesis in *Arabidopsis*. Plant Cell **16:** 2614–2628.

Bednarek, S.Y., and Backues, S.K. (2010). Plant dynamin-related protein families DRP1 and DRP2 in plant development. Biochem. Soc. Trans. **38:** 797–806.

Blackbourn, H.D., and Jackson, A.P. (1996). Plant clathrin heavy chain: Sequence analysis and restricted localisation in growing pollen tubes. J. Cell Sci. **109:** 777–786.

Bonhomme, S., Grelon, M., Guerche, P., Horlow, C., and Vezon, D. (1999). Practical Course on Genetic and Molecular Analysis of Arabidopsis. Module 1: Arabidopsis Gametogenesis. EMBO Course. http://www.isv.cnrs-gif.fr/embo99/manuals/pdf/ch1.pdf.

Borg, M., Brownfield, L., and Twell, D. (2009). Male gametophyte development: a molecular perspective. J. Exp. Bot. **60:** 1465–1478.

Boudjeko, T., Andème-Onzighi, C., Vicré, M., Balangé, A.P., Ndoumou, D.O., and Driouich, A. (2006). Loss of pectin is an early event during infection of cocoyam roots by Pythium myriotylum. Planta **223:** 271–282.

Brown, R., and Lemmon, B. (1991). Pollen development in orchids. 5. A generative cell domain involved in spatial control of the hemispherical cell plate. J. Cell Sci. **100:** 559–565.

Cecchetti, V., Altamura, M.M., Falasca, G., Costantino, P., and Cardarelli, M. (2008). Auxin regulates *Arabidopsis* anther dehiscence, pollen maturation, and filament elongation. Plant Cell **20:** 1760–1774.

Chen, X.Y., and Kim, J.Y. (2009). Callose synthesis in higher plants. Plant Signal. Behav. **4:** 489–492.

Christensen, C.A., King, E.J., Jordan, J.R., and Drews, G.N. (1997). Megagametogenesis in Arabidopsis wild type and the Gf mutant. Sex. Plant Reprod. **10:** 49–64.

Coimbra, S., Almeida, J., Junqueira, V., Costa, M.L., and Pereira, L.G. (2007). Arabinogalactan proteins as molecular markers in *Arabidopsis thaliana* sexual reproduction. J. Exp. Bot. **58:** 4027–4035.

Collings, D.A., Gebbie, L.K., Howles, P.A., Hurley, U.A., Birch, R.J., Cork, A.H., Hocart, C.H., Arioli, T., and Williamson, R.E. (2008). Arabidopsis dynamin-like protein DRP1A: A null mutant with widespread defects in endocytosis, cellulose synthesis, cytokinesis, and cell expansion. J. Exp. Bot. **59:** 361–376.

Colombo, M., Masiero, S., Vanzulli, S., Lardelli, P., Kater, M.M., and Colombo, L. (2008). AGL23, a type I MADS-box gene that controls

female gametophyte and embryo development in Arabidopsis. Plant J. **54:** 1037–1048.

Curtis, M.J., Belcram, K., Bollmann, S.R., Tominey, C.M., Hoffman, P.D., Mercier, R., and Hays, J.B. (2009). Reciprocal chromosome translocation associated with T-DNA-insertion mutation in Arabidopsis: Genetic and cytological analyses of consequences for gametophyte development and for construction of doubly mutant lines. Planta **229:** 731–745.

del Pozo, J.C., Lopez-Matas, M.A., Ramirez-Parra, E., and Gutierrez, C. (2005). Hormonal control of the plant cell cycle. Physiol. Plant. **123:** 173–183.

Derksen, J., Rutten, T., Lichtscheidl, I.K., de Win, A.H.N., Pierson, E.S., and Rongen, G. (1995). Quantitative analysis of the distribution of organelles in tobacco pollen tubes: Implications for exocytosis and endocytosis. Protoplasma **188:** 267–276.

Dhonukshe, P., Aniento, F., Hwang, I., Robinson, D.G., Mravec, J., Stierhof, Y.D., and Friml, J. (2007). Clathrin-mediated constitutive endocytosis of PIN auxin efflux carriers in Arabidopsis. Curr. Biol. **17:** 520–527.

Dhonukshe, P., et al. (2008). Generation of cell polarity in plants links endocytosis, auxin distribution and cell fate decisions. Nature **456:** 962–966.

Ferguson, C., Teeri, T., Siika-Aho, M., Read, S., and Bacic, A. (1998). Location of cellulose and callose in pollen tubes and grains of *Nicotiana tabacum*. Planta **206:** 452–460.

Fujimoto, M., Arimura, S., Nakazono, M., and Tsutsumi, N. (2007). Imaging of plant dynamin-related proteins and clathrin around the plasma membrane by variable incidence angle fluorescence microscopy. Plant Biotechnol. **24:** 449–455.

Fujimoto, M., Arimura, S., Nakazono, M., and Tsutsumi, N. (2008). Arabidopsis dynamin-related protein DRP2B is co-localized with DRP1A on the leading edge of the forming cell plate. Plant Cell Rep. **27:** 1581–1586.

Fujimoto, M., Arimura, S., Ueda, T., Takanashi, H., Hayashi, Y., Nakano, A., and Tsutsumi, N. (2010). Arabidopsis dynamin-related proteins DRP2B and DRP1A participate together in clathrin-coated vesicle formation during endocytosis. Proc. Natl. Acad. Sci. USA **107:** 6094–6099.

Geldner, N., Anders, N., Wolters, H., Keicher, J., Kornberger, W., Muller, P., Delbarre, A., Ueda, T., Nakano, A., and Jürgens, G. (2003). The Arabidopsis GNOM ARF-GEF mediates endosomal recycling, auxin transport, and auxin-dependent plant growth. Cell **112:** 219–230.

Geldner, N., Hyman, D.L., Wang, X., Schumacher, K., and Chory, J. (2007). Endosomal signaling of plant steroid receptor kinase BRI1. Genes Dev. **21:** 1598–1602.

Heese, A., Hann, D.R., Gimenez-Ibanez, S., Jones, A.M.E., He, K., Li, J., Schroeder, J.I., Peck, S.C., and Rathjen, J.P. (2007). The receptor-like kinase SERK3/BAK1 is a central regulator of innate immunity in plants. Proc. Natl. Acad. Sci. USA **104:** 12217–12222.

Hejátko, J., Pernisová, M., Eneva, T., Palme, K., and Brzobohatý, B. (2003). The putative sensor histidine kinase CKI1 is involved in female gametophyte development in Arabidopsis. Mol. Genet. Genomics **269:** 443–453.

Henley, J.R., Krueger, E.W., Oswald, B.J., and McNiven, M.A. (1998). Dynamin-mediated internalization of caveolae. J. Cell Biol. **141:** 85–99.

Herman, E.M., and Lamb, C.J. (1992). Arabinogalactan-rich glycoproteins are localized on the cell surface and in intravacuolar multivesicular bodies. Plant Physiol. **98:** 264–272.

Heslop-Harrison, J. (1968). Synchronous pollen mitosis and the formation of the generative cell in massulate orchids. J. Cell Sci. **3:** 457–466.

Jin, J.B., Kim, Y.A., Kim, S.J., Lee, S.H., Kim, D.H., Cheong, G.W., and Hwang, I. (2001). A new dynamin-like protein, ADL6, is involved in trafficking from the trans-Golgi network to the central vacuole in *Arabidopsis*. Plant Cell **13:** 1511–1526.

Johnson, S.A., and McCormick, S. (2001). Pollen germinates precociously in the anthers of raring-to-go, an Arabidopsis gametophytic mutant. Plant Physiol. **126:** 685–695.

Jones, S.M., Howell, K.E., Henley, J.R., Cao, H., and McNiven, M.A. (1998). Role of dynamin in the formation of transport vesicles from the trans-Golgi network. Science **279:** 573–577.

Kang, B.H., Busse, J.S., and Bednarek, S.Y. (2003a). Members of the *Arabidopsis* dynamin-like gene family, ADL1, are essential for plant cytokinesis and polarized cell growth. Plant Cell **15:** 899–913.

Kang, B.H., Busse, J.S., Dickey, C., Rancour, D.M., and Bednarek, S.Y. (2001). The Arabidopsis cell plate-associated dynamin-like protein, ADL1Ap, is required for multiple stages of plant growth and development. Plant Physiol. **126:** 47–68.

Kang, B.H., Rancour, D.M., and Bednarek, S.Y. (2003b). The dynamin-like protein ADL1C is essential for plasma membrane maintenance during pollen maturation. Plant J. **35:** 1–15.

Konopka, C.A., Backues, S.K., and Bednarek, S.Y. (2008). Dynamics of *Arabidopsis* dynamin-related protein 1C and a clathrin light chain at the plasma membrane. Plant Cell **20:** 1363–1380.

Konopka, C.A., and Bednarek, S.Y. (2008). Comparison of the dynamics and functional redundancy of the Arabidopsis dynamin-related isoforms DRP1A and DRP1C during plant development. Plant Physiol. **147:** 1590–1602.

Konopka, C.A., Schleede, J.B., Skop, A.R., and Bednarek, S.Y. (2006). Dynamin and cytokinesis. Traffic **7:** 239–247.

Lam, B.C., Sage, T.L., Bianchi, F., and Blumwald, E. (2002). Regulation of ADL6 activity by its associated molecular network. Plant J. **31:** 565–576.

Latrasse, D., Benhamed, M., Henry, Y., Domenichini, S., Kim, W., Zhou, D.X., and Delarue, M. (2008). The MYST histone acetyltransferases are essential for gametophyte development in Arabidopsis. BMC Plant Biol. **8:** 121.

Liu, J., et al. (2008). Targeted degradation of the cyclin-dependent kinase inhibitor ICK4/KRP6 by RING-type E3 ligases is essential for mitotic cell cycle progression during *Arabidopsis* gametogenesis. Plant Cell **20:** 1538–1554.

Michaels, S.D., and Amasino, R.M. (2001). High throughput isolation of DNA and RNA in 96-well format using a paint shaker. Plant Mol. Biol. Rep. **19:** 227–233.

Oh, P., McIntosh, D.P., and Schnitzer, J.E. (1998). Dynamin at the neck of caveolae mediates their budding to form transport vesicles by GTP-driven fission from the plasma membrane of endothelium. J. Cell Biol. **141:** 101–114.

Orth, J.D., and McNiven, M.A. (2003). Dynamin at the actin-membrane interface. Curr. Opin. Cell Biol. **15:** 31–39.

Otegui, M.S., Mastronarde, D.N., Kang, B.H., Bednarek, S.Y., and Staehelin, L.A. (2001). Three-dimensional analysis of syncytial-type cell plates during endosperm cellularization visualized by high resolution electron tomography. Plant Cell **13:** 2033–2051.

Owen, H.A., and Makaroff, C. (1995). Ultrastructure of microsporogenesis and microgametogenesis in *Arabidopsis thaliana* (L.) Heynh. ecotype Wassilewskija (Brassicaceae). Protoplasma **185:** 7–21.

Pagnussat, G.C., Alandete-Saez, M., Bowman, J.L., and Sundaresan, V. (2009). Auxin-dependent patterning and gamete specification in the Arabidopsis female gametophyte. Science **324:** 1684–1689.

Park, S.K., and Twell, D. (2001). Novel patterns of ectopic cell plate growth and lipid body distribution in the Arabidopsis gemini pollen1 mutant. Plant Physiol. **126:** 899–909.

Pischke, M.S., Jones, L.G., Otsuga, D., Fernandez, D.E., Drews,

G.N., and Sussman, M.R. (2002). An Arabidopsis histidine kinase is essential for megagametogenesis. Proc. Natl. Acad. Sci. USA **99:** 15800–15805.

Preuss, D., Rhee, S.Y., and Davis, R.W. (1994). Tetrad analysis possible in Arabidopsis with mutation of the QUARTET (QRT) genes. Science **264:** 1458–1460.

Pucadyil, T.J., and Schmid, S.L. (2008). Real-time visualization of dynamin-catalyzed membrane fission and vesicle release. Cell **135:** 1263–1275.

Sawa, S., Koizumi, K., Naramoto, S., Demura, T., Ueda, T., Nakano, A., and Fukuda, H. (2005). *DRP1A* is responsible for vascular continuity synergistically working with *VAN3* in Arabidopsis. Plant Physiol. **138:** 819–826.

Seguí-Simarro, J.M., Austin II, J.R., White, E.A., and Staehelin, L.A. (2004). Electron tomographic analysis of somatic cell plate formation in meristematic cells of *Arabidopsis* preserved by high-pressure freezing. Plant Cell **16:** 836–856.

Steinmann, T., Geldner, N., Grebe, M., Mangold, S., Jackson, C.L., Paris, S., Gälweiler, L., Palme, K., and Jürgens, G. (1999). Coordinated polar localization of auxin efflux carrier PIN1 by GNOM ARF GEF. Science **286:** 316–318.

Töller, A., Brownfield, L., Neu, C., Twell, D., and Schulze-Lefert, P. (2008). Dual function of Arabidopsis glucan synthase-like genes GSL8 and GSL10 in male gametophyte development and plant growth. Plant J. **54:** 911–923.

Twell, D., Oh, S., and Honys, D. (2006). Pollen development, a genetic and transcriptomic view. Plant Cell Monogr. **3:** 15–45.

Van Damme, D., Coutuer, S., De Rycke, R., Bouget, F.Y., Inzé, D., and Geelen, D. (2006). Somatic cytokinesis and pollen maturation in *Arabidopsis* depend on TPLATE, which has domains similar to coat proteins. Plant Cell **18:** 3502–3518.

Yao, Q., Chen, J., Cao, H., Orth, J.D., McCaffery, J.M., Stan, R.V., and McNiven, M.A. (2005). Caveolin-1 interacts directly with dynamin-2. J. Mol. Biol. **348:** 491–501.